Materials Science & Engineering A 788 (2020) 139567

Contents lists available at ScienceDirect

Materials Science & Engineering A

journal homepage: http://www.elsevier.com/locate/msea

Structure refinement, mechanical properties and feasibility of deformation of hypereutectic Al–Fe–Zr and Al–Ni–Zr alloys subjected to ultrasonic melt processing

Suwaree Chankitmunkong [a,b,*], Dmitry G. Eskin [b,c], Chaowalit Limmaneevichitr [a]

[a] Department of Production Engineering, Faculty of Engineering, King Mongkut's University of Technology Thonburi, 126 Pracha-Utid Rd., Bangmod, Tungkhru, Bangkok, 10140, Thailand
[b] Brunel University London, BCAST, Uxbridge, Middlesex, UB8 3PH, United Kingdom
[c] Tomsk State University, Tomsk, 634050, Russian Federation

ARTICLE INFO

Keywords:
Hypereutectic alloy
Al–Ni alloy
Al–Fe alloy
Ultrasonic melt processing
Precipitation hardening
Structure refinement
Hot rolling

ABSTRACT

Hypereutectic Al–Fe and Al–Ni alloys offer a potentially attractive combination of properties, e.g. high-temperature strength and stability, high elastic modulus and low coefficient of thermal expansion. This potential, however, cannot be reached unless the structure of these alloys is refined so that their processing becomes possible. In this study, we for the first time apply ultrasonic melt processing for refining the structure of hypereutectic Al-4% Fe and Al-8% Ni alloys with 0.3 wt% Zr addition. Both primary Al_3Fe and Al_3Ni particles as well as aluminum/eutectic grains are significantly refined. It is suggested that cavitation-induced fragmentation of primary Al_3Zr crystals plays a significant role in the nucleation of intermetallics as well as aluminum. Furthermore, the hardness and tensile properties of the alloys substantially increase after ultrasonic treatment due to the refined structure, which also contributes to the considerably enhanced ductility of the alloys. As a result, the fracture mode changes from brittle fracture to ductile fracture. The increase in ductility makes the alloys suitable for hot deformation, which is demonstrated by lab-scale hot rolling. In addition, precipitation hardening of the alloys can be achieved by high-temperature annealing at 450 °C due to retained Zr in the Al solid solution upon solidification. The results are supported by the analysis of the composition of a supersaturated solid solution of Zr in Al and scanning and transmission electron microscopy that confirms the precipitation of coherent Al_3Zr nanoparticles. It is demonstrated that a combination of ultrasonic melt processing and alloying with Zr makes it feasible to develop new class of hypereutectic casting and wrought alloys based on the Al–Fe and Al–Ni systems.

1. Introduction

Considerable efforts have been devoted over decades to the development of aluminum alloys of various systems because the industry requires a range of superior mechanical properties for different applications, including high-temperature and structural applications of cast and wrought products. Hypereutectic Al–Si alloys is an example of highly heterogeneous materials that are widely used as replacement of steel or cast iron due to a good combination of properties, such as low weight and thermal-expansion coefficient, high elastic modulus and wear resistance, and good castability [1]. Si, however, is a fast diffusing element and thermal stability of Al–Si alloys is limited to 200–250 °C. There is a need of increasing the working temperatures of aluminum alloys, along with improving some other important properties such as rigidity and thermal expansion. Other alloying systems that offer a heterogeneous structure along with promising combination of these properties are, therefore, under scrutiny. The development of alloys that can be also used as deformed parts is very important as it opens much wider avenues of industrial applications. Hypereutectic Al–Fe alloys were studied by Cubero-Sesin and Horita [2] and hypereutectic Al–Ni alloys by Kilicaslan and Karakose [3] as candidate materials to replace hypereutectic Al–Si alloys. These studies were, however, very limited in

* Corresponding author. Department of Production Engineering, Faculty of Engineering, King Mongkut's University of Technology Thonburi, 126 Pracha-Utid Rd., Bangmod, Tungkhru, Bangkok, 10140, Thailand.
E-mail addresses: suwaree.03@mail.kmutt.ac.th (S. Chankitmunkong), dmitry.eskin@brunel.ac.uk (D.G. Eskin), chaowalit.lim@mail.kmutt.ac.th (C. Limmaneevichitr).

https://doi.org/10.1016/j.msea.2020.139567
Received 24 January 2020; Received in revised form 13 April 2020; Accepted 11 May 2020
Available online 25 May 2020

scope and scale (severe plastic deformation, nanoindentation). There are publications demonstrating a potential of cast hypoeutectic and eutectic Al–Ni alloys for high-temperature applications, especially with additions of Zr or Sc [4–6]. In particular, Belov et al. [4,6] demonstrated that eutectic Al–Ni alloys with an addition of up to 0.8% Zr showed at least two-fold increase in the 100-h strength at 350 °C and 3-times improved creep resistance at 400 °C as compared to a piston Al–Si alloy of AA4032 type.

Moving to hypereutectic alloys may improve the properties further but this opportunity can only be realized if the structure of the alloys is refined so that the alloys acquire some ductility. The mechanical properties of these alloys typically depend on the size and distribution of primary intermetallics such as Al_3Fe and Al_3Ni. The high elastic modulus and good mechanical properties at elevated temperatures of Al–Fe and Al–Ni alloys were reported elsewhere [7]. In this work the small-scale samples were swage rolled to obtain samples. Young's modulus (at room temperature) was 79.5 GPa and 85.7 GPa and the tensile strength (at 300 °C) was 43 MPa and 51 MPa for rolled Al–4.8 wt% Fe and Al–9.5 wt% Ni alloys, respectively.

Obviously, the large size of intermetallics leads to the significant reduction of ductility and tensile strength through crack initiation [8]. It is reported that the hypereutectic alloys of Al–Fe and Al–Ni systems cannot be deformed unless the primary particles are refined or fragmented, e.g. by helical (swage) rolling [9]. More recently, it was suggested that the mechanical properties of hypereutectic Al–Fe could be improved through the modification of brittle Fe intermetallic by rare earth additions [10]. To the best of our knowledge, there are no reports where the structure of these alloys has been refined via liquid metal processing.

One of the known methods to refine primary intermetallics is ultrasonic melt processing (USP) [11] with benefits of improving the strength and ductility of the alloy [12]. The main mechanisms of intermetallic refinement using USP are known to be through enhanced nucleation and fragmentation as a result of melt cavitation [12]. In our previous work, we reported that the USP applied in different temperature ranges during solidification significantly refined dendrites and intermetallics in near-eutectic Al–Si alloys [13]. It was also reported that the USP application could improve the tensile properties by modification the morphology of primary Fe-intermetallic particles [14]. USP has not been, however, applied before to the refinement of structure of hypereutectic A–Fe and Al–Ni alloys.

Structure refinement in solid-solution type Al alloys (typically wrought alloys) upon USP can be considerably enhanced by additions of Zr [15], which is related to the refinement of primary Al_3Zr particles so that they become efficient nucleation sites for Al [16]. This effect has not been previously tested in hypereutectic Al–Fe and Al–Ni alloys. On the other hand, additions of transition elements such as Zr are known to improve the properties of Al alloys through high-temperature precipitation of Al_3Zr ($L1_2$) nano-particles, this hardening effects being quite stable up to 400–450 °C [17]. Precipitation hardening at 400–450 °C of a eutectic Al–6% Ni alloy with an addition of 0.5% Zr was previously demonstrated by Belov et al. [18], who reported the stability of properties acquired upon heat treatment up to 350–400 °C. However, such a large amount of Zr required very high casting temperatures (850 °C).

Nevertheless, there might be a potential for further performance improvement of heterogeneous hypereutectic alloys through high-temperature precipitation hardening.

Our literature survey shows that there is only limited amount of research available on hypereutectic Al–Fe and Al–Ni alloys, let alone the application of USP and additional alloying on microstructure, hardening and deformability of these alloys. The principle novelty of this study lies in the application of USP in combination with Zr for achieving the combined effect of structure refinement and hardening in a new class of materials, e.g. hypereutectic Al–Ni and Al–Fe alloys. The results allow one to unleash the potential of these alloys as structural materials for both casting and wrought applications.

Therefore, this work is focused on the three main objectives. The first objective is to understand the effect of USP and Zr on microstructural evolution during solidification in hypereutectic Al-4% Fe and Al-8% Ni alloys, which has not been studied before. The second objective is to assess the effects of the structure refinement and hardening by Zr on the mechanical properties, which has not been explored in these alloys before. And the third one is to study the feasibility of subsequent forming of such alloys. It is important to note that this is a feasibility study and the studied alloys are model materials (binary with small addition of Zr), hence their properties need to be taken in comparison rather than in absolute values when compared to the commercial multi-component alloys. Same applies to the deformation as we just wanted to reveal the potential of the alloys to deformation rather than develop a deformation routine for those alloys, which is well beyond the scope of this paper.

2. Experimental procedure

The ThermoCalc software with the Scheil model (TCAL4 database) was used to calculate the sequence of phase formation and define the temperature ranges for ultrasonic melt processing (USP) upon casting. The chemical compositions of Al-4 wt% Fe-0.3 wt% Zr (Al4Fe0·3Zr) and Al-8 wt% Ni-0.3 wt% Zr (Al8Ni0·3Zr) were used to simulate the alloy systems (here and below only wt% are used).

The experimental alloys were prepared in an electric furnace from commercially pure (99.9%) aluminum, Al–11.7% Ni, Al-10% Fe, and Al-6% Zr master alloys. The alloys were prepared in clay-graphite crucibles at 780 °C, the melt volume was 0.5 kg for a cylindrical mold and 2 kg for a slab mold. The nominal compositions were analyzed by Foundry Master optical emission spectrometer, and given in Table 1.

Firstly, the Al4Fe and Al8Ni alloys with and without 0.3 wt% Zr addition were cast in a cylindrical steel mold (25 mm diameter, 100 mm high) to investigate the effect of USP with regard to the temperature range of processing and the presence of Zr. The alloys without USP treatment were poured at 730 °C for Al–Fe alloys and 680 °C for Al–Ni alloys. The USP was performed in the crucible in temperature ranges of 780–750 °C and 780-730 °C for hypereutectic Al–Fe alloys (Al4Fe and Al4Fe0·3Zr alloy), and in temperature ranges of 740–720 °C and 740-680 °C for hypereutectic Al–Ni alloys (Al8Ni and Al8Ni0·3Zr alloys), respectively. The temperatures were selected to cover the primary solidification range of Al_3Zr. The melt was poured into the mold after the end of USP (or at 730 °C in the case of a higher temperature).

In the second series of experiments, the alloys were cast in a slab mold (170 mm × 190 mm × 17 mm in dimensions) with USP performed in temperature ranges of 780–730 °C and 740-710 °C for Al4Fe0·3Zr and Al8Ni0·3Zr alloys, respectively. The alloys were poured immediately after the end of USP. The Al4Fe0·3Zr alloys and Al8Ni0·3Zr alloys without USP were poured at temperatures of 730 °C and 710 °C, respectively. The higher pouring temperature was selected to assure full mold filling.

Ultrasonic melt processing was performed by dipping a pre-heated (600 °C) niobium sonotrode 20 mm in diameter into the melt in the crucible by approximately 5 mm below the melt surface prior to casting.

Table 1
Chemical compositions of Al4Fe and Al8Ni alloys with/without 0.3% Zr addition as determined by optical emission spectrometry.

Casting	Alloys	Chemical compositions (wt %)			
		Zr	Ni	Fe	Al
Cylindrical mold	Al4Fe-1	<0.0001	<0.001	4.15	95.85
	Al4Fe0·3Zr-1	0.29	<0.001	4.10	95.62
	Al8Ni-1	<0.001	7.98	<0.001	92.02
	Al8Ni0·3Zr-1	0.30	8.1	<0.001	91.6
Slab mold	Al4Fe0·3Zr-2	0.29	<0.001	4.13	95.58
	Al8Ni0·3Zr-2	0.31	7.98	<0.001	91.74

A Reltec water-cooled magnetostrictive transducer with a driving frequency of 17.5 kHz powered the sonotrode with an amplitude at the tip of the sonotrode being at least ±20 μm.

The cast slabs were subsequently deformed by a hot rolling process. The specimens were heated to 400 °C, and then the slab with an initial thickness of 17 mm was rolled in a lab-scale rolling mill in steps of 10% reduction until reaching 50% reduction. Intermediate re-heating was applied.

Samples for metallographic examination were taken from the center of the castings to avoid the chill-zone effect, then the structures of as-cast and hot-rolled samples were examined using optical microscopy (OM, Zeiss Axio Scope.A1) and scanning electron microscopy (SEM, ZEISS Supra 35). The deformed samples were also investigated in three directions of deformation (top, side and cross section). The standard method of grinding was applied for the preparation of samples, then the surface was etched by ferric chloride dissolved in water to observe macrostructure. For microstructure analysis, the samples were polished using standard techniques. Selected samples were also anodized in Barker's solution (5% HBF_4 water solution) for about 2 min at 20 VDC and were then examined in OM under polarized light. The average grain sizes and the average size of intermetallics (with an exception of individual large particles) were measured in the center of cylindrical and slab samples using the linear intercept method according to ASTM E112-10. The quantitative analysis was conducted by at least 30 measurements from different 20 images for each sample, and the average values were used to represent the grain and intermetallic sizes. Furthermore, the amount of Zr in the supersaturated Al matrix and the precipitation of Al_3Zr after aging were analyzed with a ZEISS Supra 35 SEM with an energy dispersive spectroscopy (EDS). Transmission electron microscopy (TEM, JEOL-2100) was used to investigate the Al_3Zr precipitates in the microstructure.

Hardness test was conducted by using a Brinell hardness tester with 187.5 N load, 5 mm ball indenter, and 20 s dwell time. The hardness was measured on as-cast and aged at 450 °C samples every 5 h for 30 h to obtain the saturated hardness values of the alloys. The hardening temperature was selected following the reference work reporting that the peak hardness occurred at 400–450 °C through the precipitation of Al_3Zr ($L1_2$) [19].

The tensile properties were measured for the as-cast and annealed specimens. The samples were machined to sub-size round tensile specimens with the 6-mm diameter and 30-mm gauge length following the ASTM standard, and then were annealed at 450 °C for 20 h (the saturated value of hardness). Tensile testing was performed in a universal testing machine Instron 5500. An extensometer with a gauge length of 50 mm was applied for the monitoring of the strain with a constant ramp rate of 1 mm/min until the specimen failed. The average values of the ultimate tensile strength (UTS), yield strength (YS) and percentage of elongation (%El) were calculated from three specimens to obtain statistical values for each condition. After testing, the fractures were examined in the SEM to analyze the failure behavior.

3. Results

3.1. A feasibility study of USP and Zr effects on hypereutectic Al4Fe and Al8Ni alloys

3.1.1. Solidification sequence in Al8Fe and Al4Ni alloys with 0.3 wt% Zr addition

Thermo-Calc software was utilized to define the solidification sequence and the temperature ranges of phase formation in hypereutecticAl4Fe and Al8Ni alloys with 0.3% Zr addition as demonstrated in Fig. 1.

The result showed that the primary Al_3Zr phase was formed in the Al4Fe0·3Zr alloy in the temperature range 772–750 °C, while in the Al4Fe0·3Zr alloy this range was lower, 730-688 °C. Furthermore, the primary Al_3Fe and Al_3Ni phases were formed later in the temperature ranges 750-655 °C and 688-646 °C, respectively. The USP temperature ranges have been selected accordingly as 780-730 °C and 740–680 °C for Al4Fe0·3Zr and Al4Fe0·3Zr alloy, respectively. These temperature ranges cover the solidification range of primary Al_3Zr solidification. These temperature ranges (as well as higher temperature ranges that included USP applied to the single-phase liquid as well) were used for casting in the cylindrical mold as described in Experimental.

3.1.2. Macrostructure upon USP treatment in the cylindrical mold

The macrostructure of the Al4Fe alloy changed somewhat by USP as shown in Fig. 2 (a-c) with some modest structure refinement achieved when USP had been performed at 780-730 °C (Fig. 2(c)). This temperature range includes the upper part of the primary Al_3Fe solidification range (see Fig. 1(a)). A higher USP temperature range (780–750 °C) did not result in structure refinement. Note that "grains" that are visible in Fig. 2 and other figures below are actually a mixture of aluminum dendrites and eutectic colonies as all the alloys are hypereutectic.

Fig. 3(a-c) shows the macrographs of the Al8Ni alloy without 0.3% Zr addition after USP performed in different temperature ranges. Results are qualitatively similar to those on Al4Fe alloys. USP of the alloys without Zr refined somewhat the structure, though it was not able to eliminate the columnar zone, which testified to an insufficient number of nucleating substrates (or crystal fragments) ahead of the solidification front. Table 2 summarizes the results by giving quantitative data for the best combination of composition and USP.

Addition of Zr (Figs. 2d and 3d) did not bring about any significant effect. When USP is applied along with the Zr addition, the structure changes dramatically with very strong refining effect clearly observed in Figs. 2e and f and 3 e, f).

Fig. 4 shows in more details how the USP and Zr additions changed

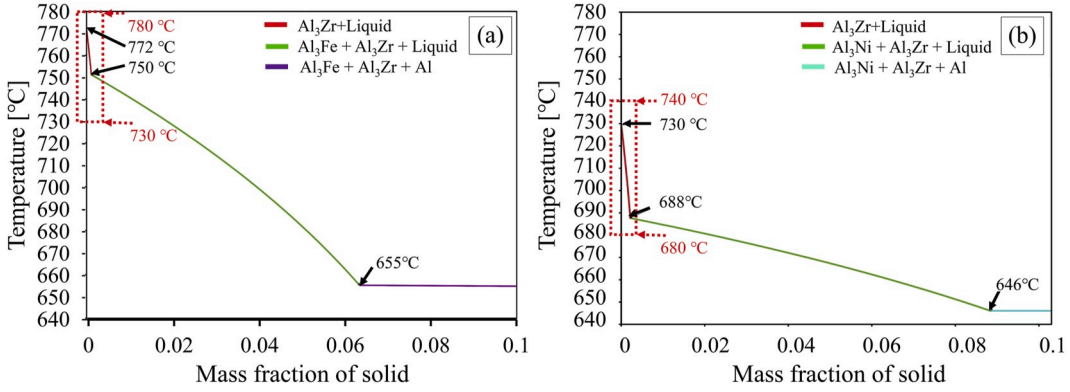

Fig. 1. ThermoCalc calculation of Scheil solidification of hypereutectic Al4Fe and Al8Ni alloys with 0.3% Zr. (a) Al4Fe0·3Zr and (b) Al8Ni0.3Zr. The temperature ranges of efficient USP, i.e. 780-730 °C and 740-680 °C, are shown by dotted lines.

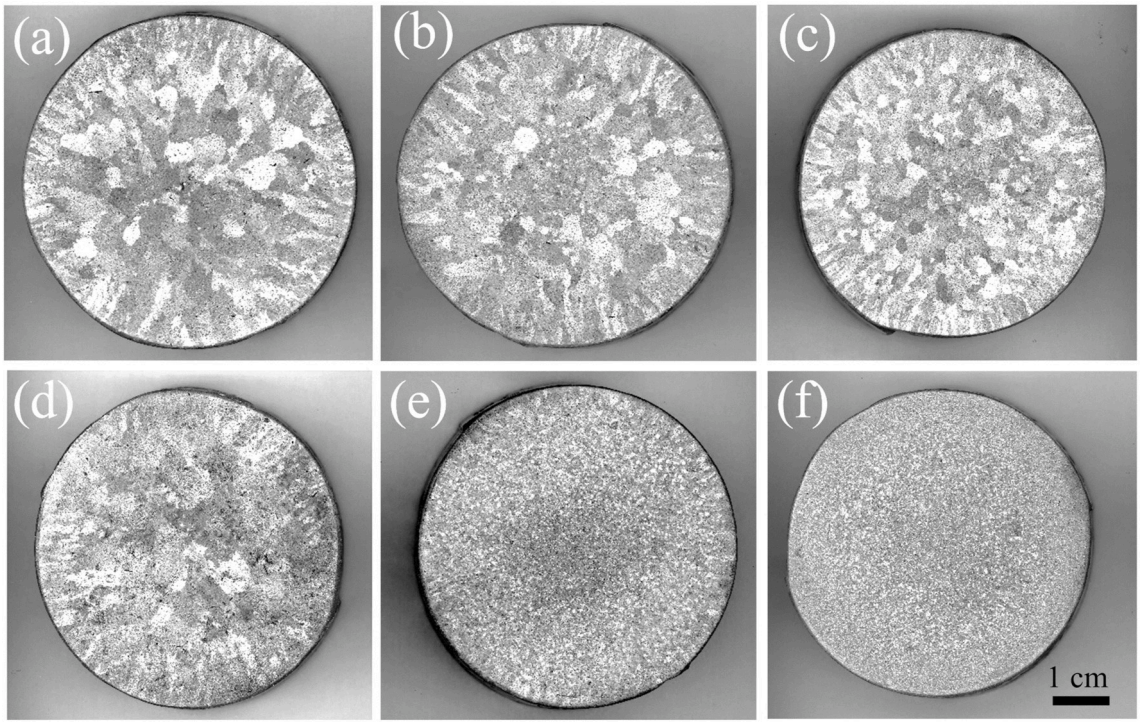

Fig. 2. Macrographs of the Al4Fe alloy (a–c), and Al4Fe0·3Zr alloy (d–f). The alloys were cast at different pouring temperatures (T_p) and USP temperature ranges (T_{USP}); (a) Al4Fe-T_p = 730 °C -No USP, (b) Al4Fe-T_{USP} = 780-750 °C, (c) Al4Fe-T_{USP} = 780-730 °C, (d) Al4Fe0·3Zr-T_p = 730 °C-No USP, (e) Al4Fe0·3Zr-T_{USP} = 780-750 °C and (d) Al4Fe0·3Zr-T_{USP} = 780-730 °C.

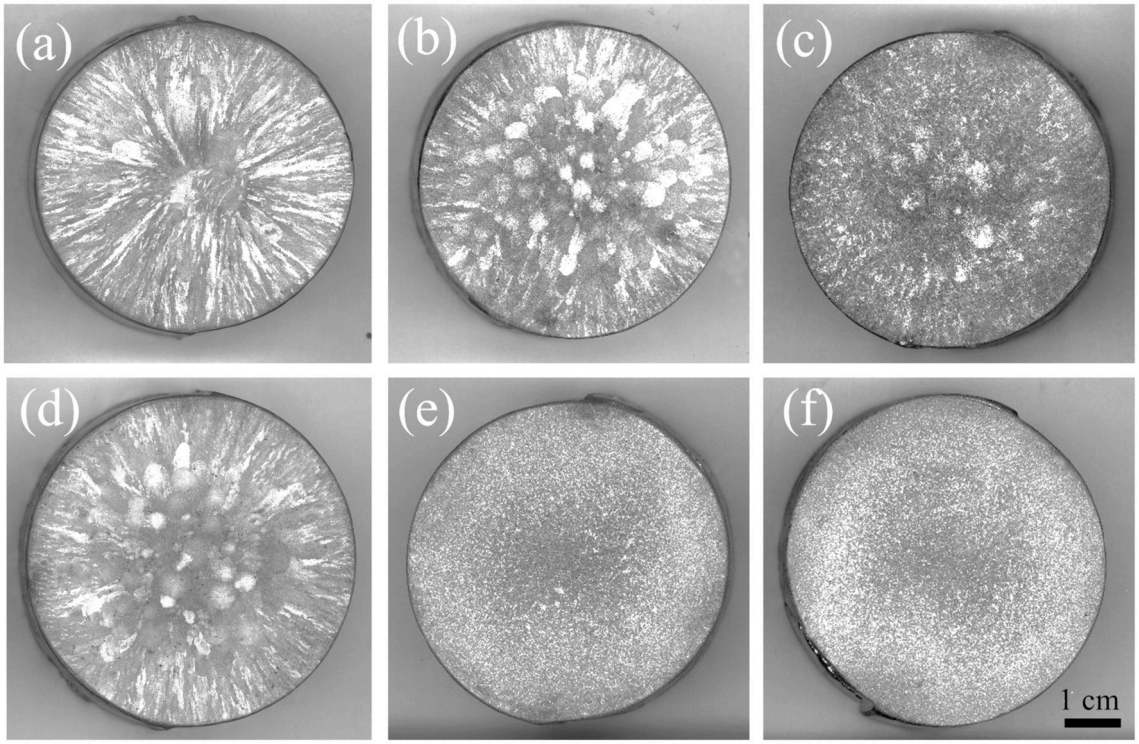

Fig. 3. Macrographs of the Al8Ni alloy (a–c), and the Al8Ni0·3Zr alloy (d–f). The alloys were cast at different pouring temperatures (T_p) and USP temperature ranges (T_{USP}); (a) Al8Ni-T_p = 680 °C-No USP, (b) Al8Ni-T_{USP} = 740-720 °C, (c) Al8Ni-T_{USP} = 740-680 °C, (d) Al8Ni0·3Zr-T_p = 680 °C-No USP, (e) Al8Ni0·3Zr-T_{USP} = 740-720 °C and (f) Al8Ni0·3Zr-T_{USP} = 740-680 °C.

the "grain" structure in the Al4Fe0·3Zr and Al8Ni0·3Zr alloys. USP made the "grains" much finer and more uniformly equiaxed. As Table 2 shows there is a significant decrease in the "grain" size with the values 194 ± 3 μm and 266 ± 5 μm achieved for the Al4Fe0·3Zr-1 and Al8Ni0·3Zr-1 alloys, respectively. This is about 3.5–4 times smaller than in the alloys not treated with ultrasound. These results confirm the macrostructure

Table 2
Quantitative results for sizes of "grains" and Al_3Fe and Al_3Ni intermetallics formed under different conditions. (only the average values of the bulk of primary intermetallics are given, with an exception of individual large particles, see Supplemental material for particle size distribution curves).

Casting	Alloys	Conditions	"Grain" size (μm)	Intermetallic size, Al_3Fe or Al_3Ni (μm)
Cylindrical mold	Al4Fe0·3Zr-1	No USP (T_p = 730 °C)	830 ± 16	159 ± 2
		USP (T_{USP} = 780-730 °C)	194 ± 3	45 ± 0.1
	Al8Ni0·3Zr-1	No USP (T_p = 680 °C)	978 ± 24	39 ± 0.3
		USP (T_{USP} = 740-680 °C)	266 ± 5	34 ± 0.3
Slab mold	Al4Fe0·3Zr-2	No USP (T_p = 730 °C)	138 ± 3	135 ± 2
		USP (T_{USP} = 780-730 °C)	99 ± 2	52 ± 0.3
	Al8Ni0·3Zr-2	No USP (T_p = 710 °C)	195 ± 4	51 ± 0.8
		USP (T_{USP} = 740-710 °C)	153 ± 4	37 ± 0.3

observations.

3.1.3. *Microstructure upon USP treatment in the cylindrical mold*

The main microstructure features of the hypereutectic alloys are, of course, primary intermetallics and eutectic colonies. Fig. 5 shows that the primary phases (Al_3Fe or Al_3Ni) were refined by USP in the presence of Zr. For the Al4Fe0·3Zr alloy, this refinement is almost by 70% (159 ± 2 μm to 45 ± 0.1 μm) as shown in Table 2. On the other hand, the average size of primary Al_3Ni crystals has not changed significantly, only from 39 ± 0.3 to 34 ± 0.3 μm, but as it is shown in Supplemental Material, individual large particles have been eliminated by USP.

In this stage of this feasibility study, it is clearly demonstrated that the combination of USP and the addition of Zr to hypereutectic Al4Fe and Al8Ni alloys effectively refines the macro- and microstructure. Neither USP nor Zr applied separately has any significant refining effect. The temperature of the USP should encompass the primary solidification range of the Al_3Zr phase and could also include an upper part of the primary solidification range of the main intermetallic phase. Based on these results, the next sections will explore the potential of hypereutectic alloys for hardening and deformation. Alloys cast in the slab mold will be considered from now on.

3.2. *Validation of structure refinement upon USP of Al4Fe0·3Zr and Al8Ni0·3Zr alloys cast in a slab mold*

Slab mold offers a possibility to produce larger castings that can be subsequently rolled. Therefore, we need to verify first if the refining effects observed in a smaller cylindrical mold and reported in the previous section can be retained in a larger casting. The Al4Fe0·3Zr-2 and Al8Ni0·3Zr-2 alloys (Table 1) were subjected to USP in temperature ranges of 780–730 °C and 740-710 °C, respectively, which was slightly higher than we considered in the previous section. This correction of the pouring temperature was necessary to assure the filling of a larger slab mold and to avoid unnecessary casting defects. However, these temperatures were within the primary temperature range of Al_3Zr (see Fig. 1), which was essential for the observed effects.

Fig. 6 confirms the findings of the previous section and demonstrates refinement of primary intermetallics upon USP, from 135 to 52 μm and from 51 to 37 μm for Al_3Fe and Al_3Ni, respectively, as shown in Table 2. Moreover, the microstructure showed that the size and spatial distribution of primary crystals became more uniform with USP applied, with less particles being significantly larger than the average (see Supplementing Materials).

Fig. 7 clearly demonstrates that the application of USP to the alloys also effectively refined the "grains" (combination of aluminum dendrites and eutectic colonies). It is most likely related to the nucleation ability of USP-refined Al_3Zr primary crystals as it is elaborated in the following observations. Fig. 8 shows the location of small primary Al_3Zr crystals in the overall microstructure. These Al_3Zr particles are either located in the center of eutectic colonies or are linked to Al_3Fe and Al_3Ni primary intermetallics. This is further illustrated at a higher magnification in Fig. 9:

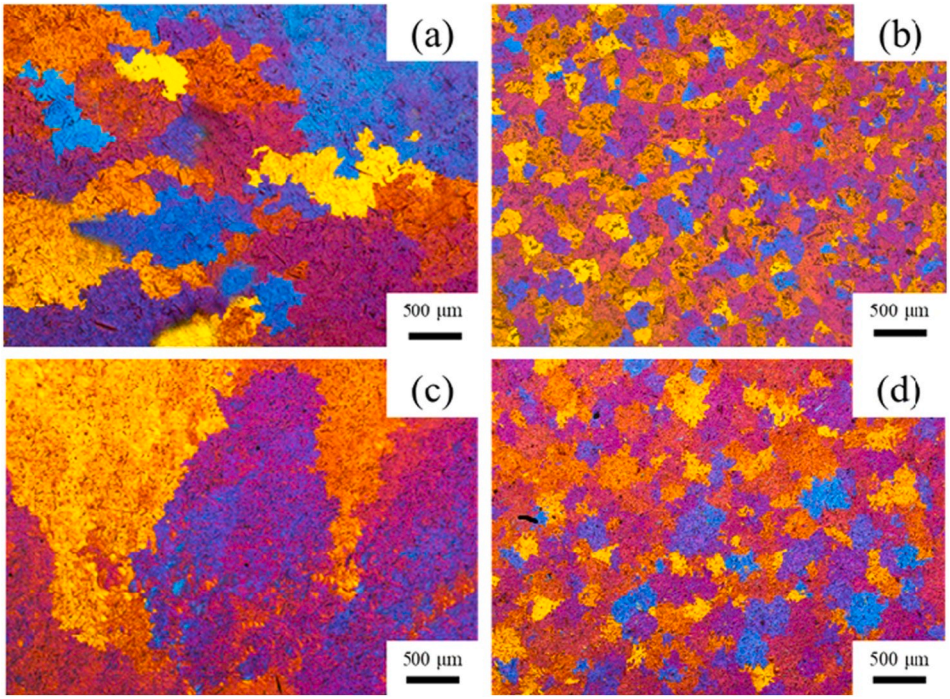

Fig. 4. Structure refinement in hypereutectic Al4Fe0·3Zr and Al8Ni0·3Zr alloys solidified in the cylindrical mold with and without USP at specific pouring (T_p) and USP temperatures (T_{USP}): Al4Fe0·3Zr-1: (a) T_p = 730 °C -No USP, (b) T_{USP} = 780-730 °C, and Al8Ni0·3Zr-1: (c) T_p = 680 °C -No USP, (d) T_{USP} = 740-680 °C.

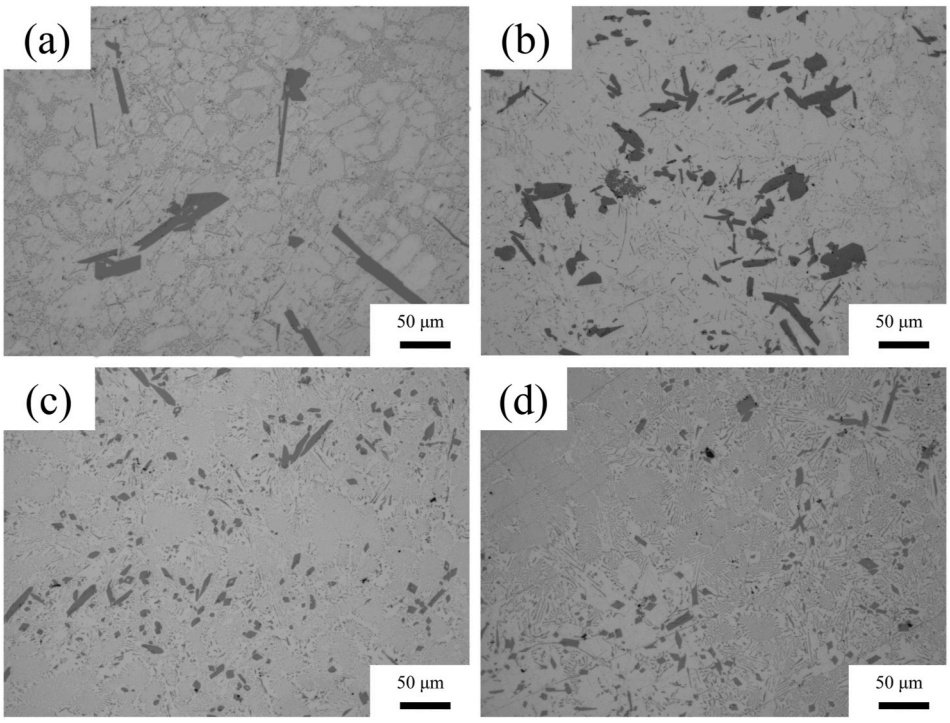

Fig. 5. Intermetallic formation in Al4Fe0·3Zr and Al8Ni0·3Zr alloys solidified in the cylindrical mold at different pouring (T_p) and USP temperatures (T_{USP}): Al4Fe0·3Zr-1: (a) T_p = 730 °C-No USP, (b) T_{USP} = 780-730 °C, and Al8Ni0·3Zr-1: (c) T_p = 680 °C-No USP, (d) T_{USP} = 740-680 °C.

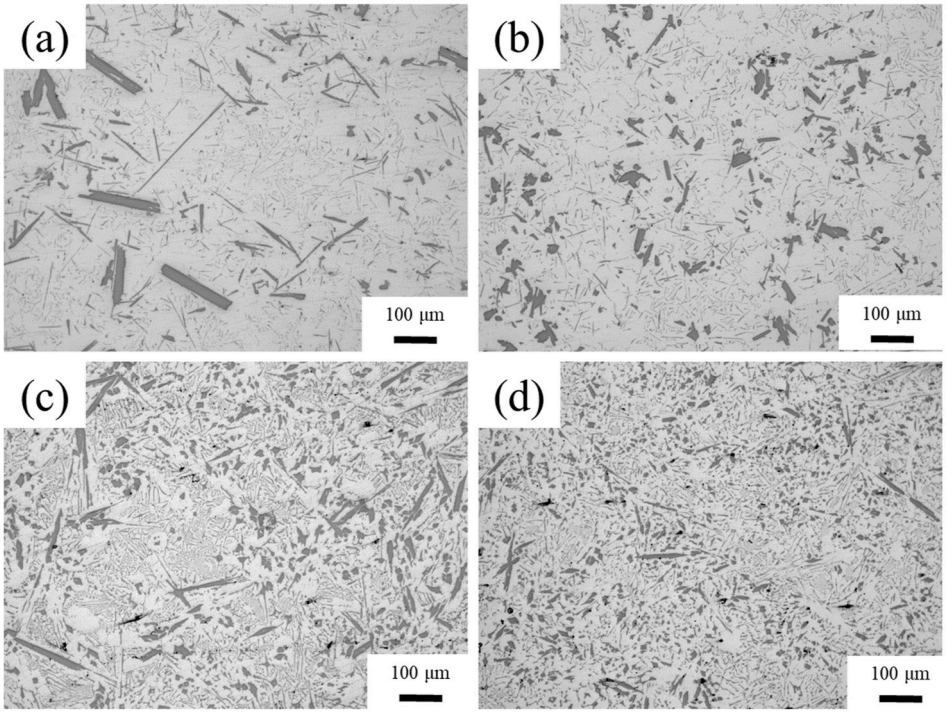

Fig. 6. Microstructure of Al4Fe0·3Zr-2 and Al8Ni0·3Zr-2 alloys solidified in the slab mold without and with USP: (a) Al4Fe0·3Zr-No USP at T_p = 730 °C, (b) Al4Fe0·3Zr-USP at T_{USP} = 780-730 °C, (c) Al8Ni0·3Zr-No USP at T_p = 710 °C and (d) Al8Ni0·3Zr-USP at T_{USP} = 740-710 °C.

Fig. 9(b) shows an Al_3Zr particle associated with an Al_3Fe intermetallic, while Fig. 9(c) shows that an Al_3Zr crystal occurs in the center of an Al dendrite that constitutes part of a eutectic colony.

3.3. *Precipitation hardening in hypereutectic Al–Fe and Al–Ni alloys with Zr addition*

Addition of Zr to an Al alloy opens an opportunity for hardening using precipitation of metastable Al_3Zr particles. This effect is well known for Al solid solution-type alloys but has not been previously

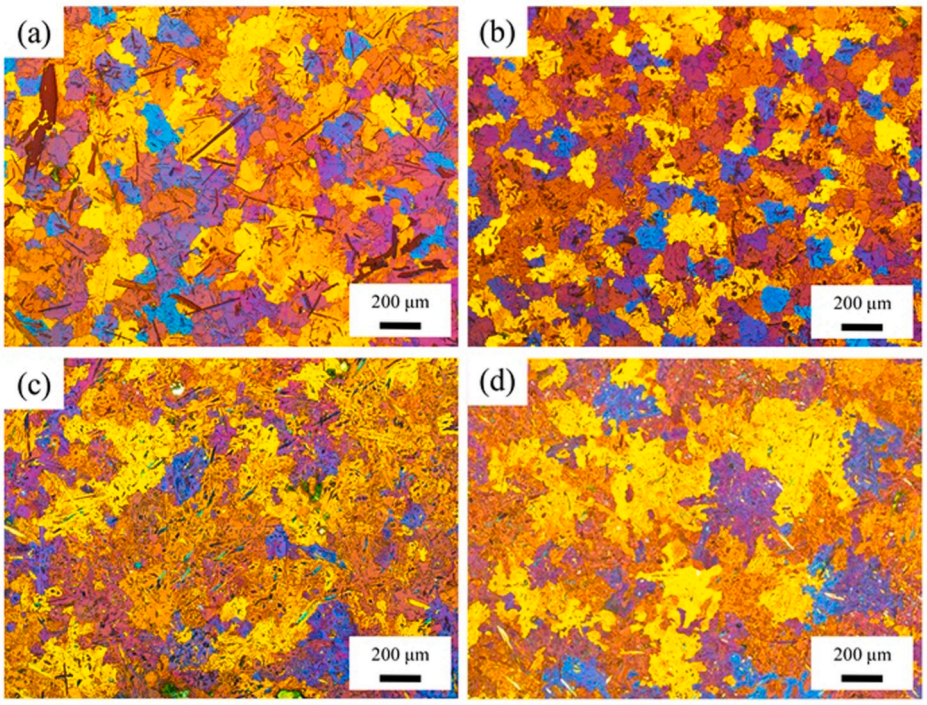

Fig. 7. "Grain" structure of Al4Fe0·3Zr-2 and Al8Ni0·3Zr-2 alloys solidified in the slab mold without and with USP: (a) Al4Fe0·3Zr-No USP at T_p = 730 °C, (b) Al4Fe0·3Zr-USP at T_{USP} = 780-730 °C, (c) Al8Ni0·3Zr-No USP at T_p = 710 °C and (d) Al8Ni0·3Zr-USP at T_{USP} = 740-710 °C.

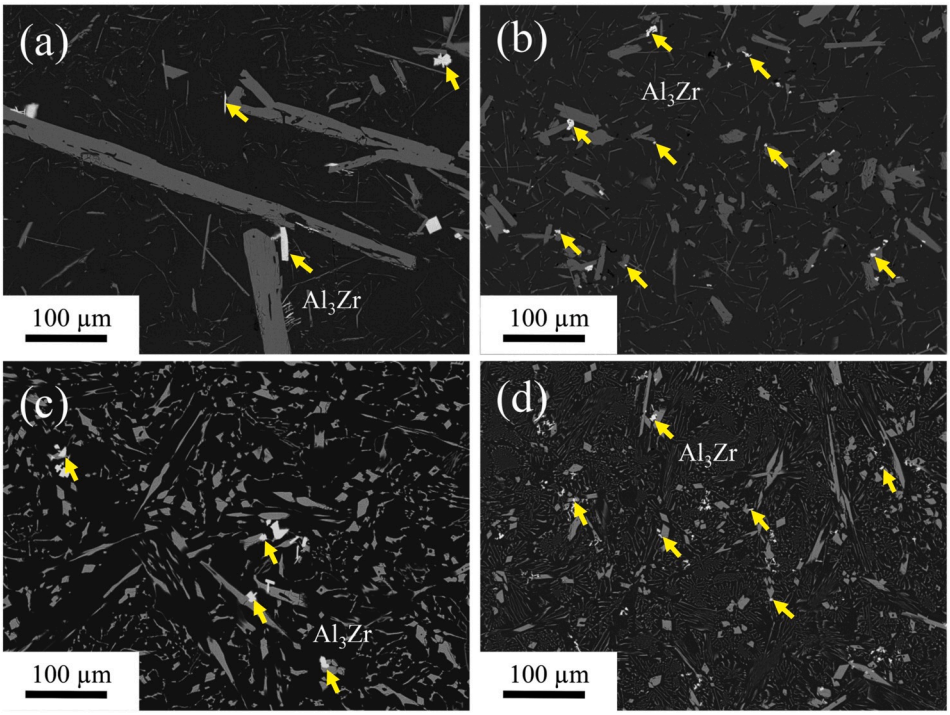

Fig. 8. SEM images showing the interaction between primary Al_3Zr crystals and other phases in the alloys with and without USP: (a) Al4Fe0·3Zr-2 without USP, (b) Al4Fe0·3Zr-2 with USP, (c) Al8Ni0·3Zr-2 without USP and (d) Al8Ni0·3Zr-2 with USP.

achieved on hypereutectic alloys. Fig. 10 shows the hardness variation of two experimental alloys annealed at 450 °C for up to 30 h. One can see that the alloys, especially Al4Fe0·3Zr, underwent precipitation hardening with the hardness increment after aging for 30 h from 35 HB to 50 HB for the Al4Fe0·3Zr alloy (Fig. 10(a)) and from 44–46 HB to 50–53 HB for the Al8Ni0·3Zr alloy (Fig. 10 (b)). Moreover, it can be seen that the hardness values stabilized after 20 h and reached the saturated level with a value around 50 HB.

Fig. 11 (a) gives the comparison of the calculated maximum Zr content that can dissolve in Al after solidification (the value reflects the solubility of Zr at the solidus temperature of the alloy) and the measured results of Zr concentration in the as-cast experimental alloys. Firstly, the

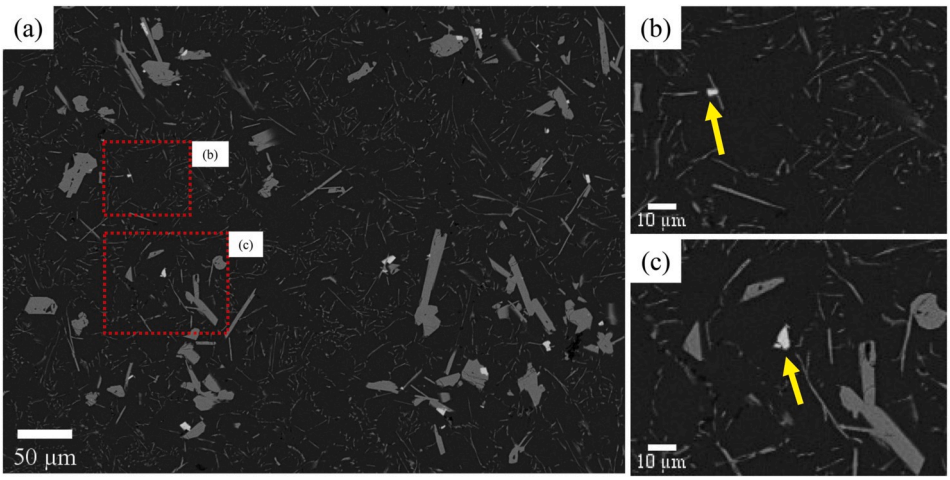

Fig. 9. SEM (back-scattered electron) images of phases in the Al4Fe0·3Zr alloy: (a) Al_3Zr (bright) and Al_3Fe (gray) phases formed in the microstructure, (b) Al_3Zr acts as a nucleation site for Al_3Fe, and (c) Al_3Zr acts as a nucleation site for aluminum (Al_3Zr pointed by yellow arrow in (b) and (c)). (For interpretation of the references to colour in this figure legend, the reader is referred to the Web version of this article.)

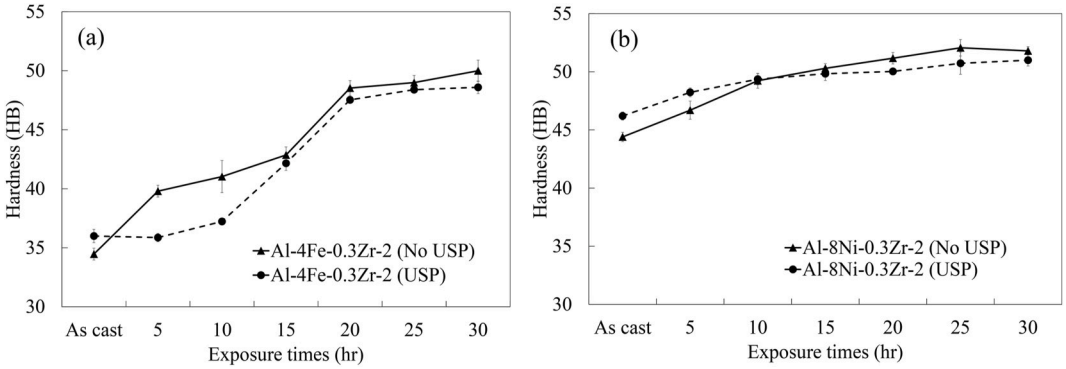

Fig. 10. Hardness variation in the alloys during heat treatment at 450 °C, at different exposure times: (a) Al4Fe0·3Zr-2 and (b) Al8Ni0·3Zr-2.

calculated result shows that the amount of Zr potentially dissolved in Al under equilibrium condition is about 0.26 and 0.24% Zr for the Al4Fe0·3Zr and Al8Ni0·3Zr alloys, respectively. The factual concentration of Zr in the Al solid solution is smaller due to the formation of primary Al_3Zr particles and the moderate cooling rate upon solidification. USP further decreases the amount of Zr in the solid solution by promoting the formation of primary Al_3Zr intermetallics.

The formation of metastable Al_3Zr precipitates upon annealing was confirmed by SEM and TEM studies and the results showed the presence and uniform distribution of Al_3Zr nano-precipitates in Al-grains as pointed by yellow arrows in Fig. 11(b). In further analysis, the HRTEM was used to observe the coherence of these precipitates with Al matrix in the aged samples. The corresponding FFT pattern identified the Al_3Zr precipitate with $L1_2$ structure, as shown in Fig. 11(c).

3.4. Tensile properties and fracture analysis

Fig. 12 demonstrates the tensile properties of as-cast and heat-treated alloys. In general, the tensile properties of both Al4Fe0·3Zr (Fig. 12(a)) and Al8Ni0·3Zr alloys (Fig. 12(b)) increased with USP and aging treatment. In the as-cast Al4Fe0·3Zr alloy, USP increased UST by 57% and YS by 14%. It is also worth noting that there was a very significant improvement in elongation, by more than 500%. After the alloy was aged at 450 °C for 30 h, it gained about 10 MPa in strength with the subsequent decrease of ductility that, nevertheless, remained considerably improved (>4%) as compared with the alloy not subjected to USP. Similar trend was observed for the Al8Ni0·3Zr alloy, where USP and aging benefited the properties of alloy, though not to the same degree as in the Al4Fe0·3Zr alloy.

The failure mechanism of the Al4Fe0·3Zr alloy was analyzed through optical micrographs images of sample cross-sections through the fracture region (Fig. 13 (a-d)). Clearly, the Al_3Fe intermetallics were the main crack initiators in the microstructure of the alloy that was not treated by USP. However, after the alloy was subjected to USP the fracture occurred through the Al phase that demonstrated the prevalence of plastic deformation (Fig. 13(b)). SEM fractography was used to analyze the failure mechanism in the Al8Ni0·3Zr alloy as can be seen in Fig. 13 (e-h). In general, the trend of tensile properties in the as-cast condition for the Al8Ni0·3Zr alloy was similar to Al4Fe0·3Zr.

One of the potential advantages of hypereutectic alloys is the improved rigidity that is characterized by an elastic modulus. We have assessed the engineering elastic modulus from the tensile curves and the results are given in Fig. 14. The results demonstrate that the improvement in strength and hardness coincided with the high elastic modulus. Moreover, it is also worth noting that the alloys that were treated by USP had higher elastic modulus in both as-cast and aged conditions as shown in Fig. 14. The maximum elastic moduli achieved were between 80 and 82 GPa, which is in agreement with reference date [7] and also higher than the elastic moduli of wrought Al alloys (69–72 GPa) and hypereutectic Al–Si alloys (75–78 GPa).

3.5. Feasibility of hot forming

Considerable improvement in ductility of the hypereutectic alloys

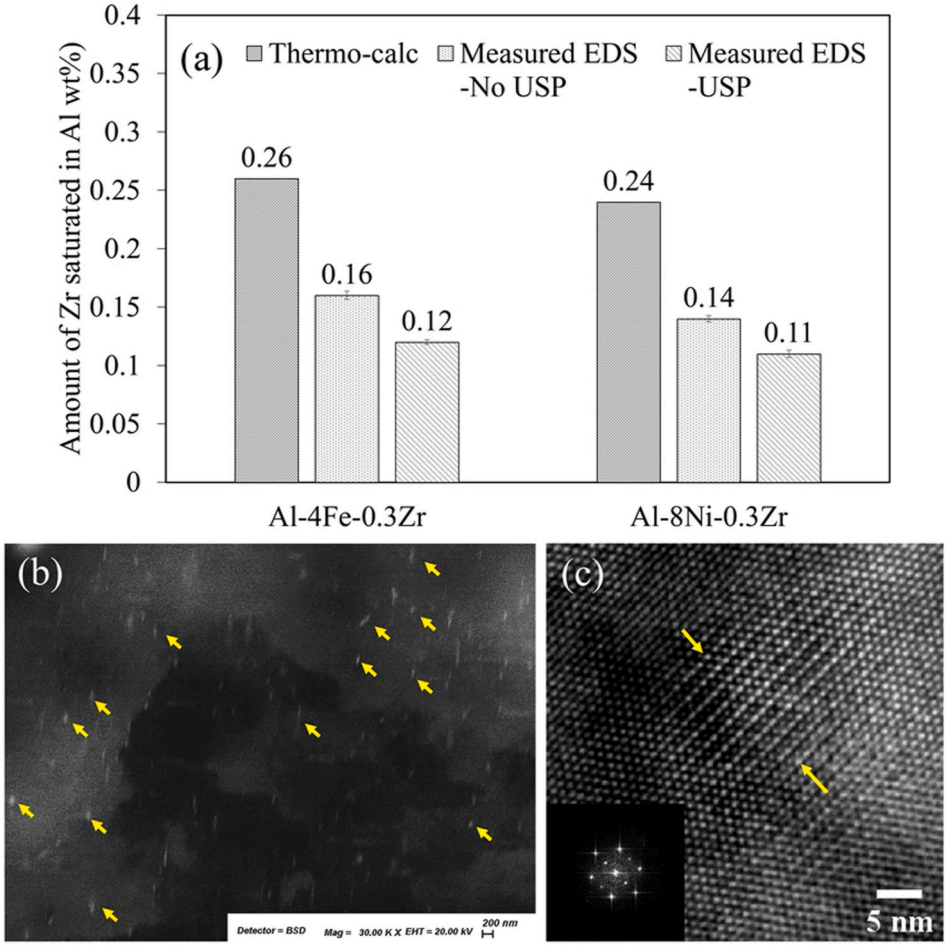

Fig. 11. The calculated (ThermoCalc) and measured concentration of Zr in the Al matrix in the Al4Fe0·3Zr and Al8Ni0·3Zr alloys with and without USP (a). (b) SEM image of Al_3Zr precipitates in the Al4Fe0·3Zr alloy with USP after holding at 450 °C for 30 h and (c) a high resolution TEM (HRTEM) image showing a coherent metastable Al_3Zr precipitate with the FFT pattern is given in the inset.

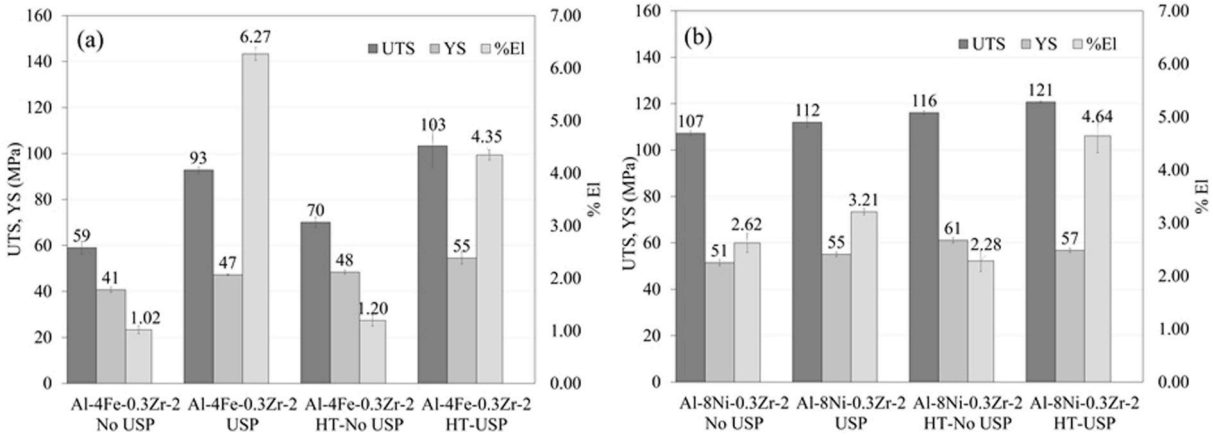

Fig. 12. Average values of mechanical properties (UTS, YS, %El) at room temperature for as-cast and heat-treated (450 °C, 30 h (HT)) alloys without and with USP: (a) Al4Fe0·3Zr alloy and (b) Al8Ni0·3Zr alloy.

containing Zr after USP makes it potentially possible to use these alloys as deformable. The specific technology of working these alloys as well as most suitable techniques of deformation, i.e., forging, hot rolling or extrusion, are well beyond the scope of this paper. Here we only demonstrate the possibility of deformation of these otherwise brittle alloys.

Fig. 15 shows that the edge cracks occurred during hot rolling and the alloys subjected to USP were less prone to forming these cracks. In fact, the rolled Al4Fe0·3Zr alloy (Fig. 15 (b)) had no edge and surface cracks at all.

The microstructure of the deformed specimens was reconstructed in three planes as shown in Fig. 16. The "grains" were elongated in the rolling direction and did not seem to be recrystallized. The deformed Al4Fe0·3Zr alloy cast without USP contained cracks associated with

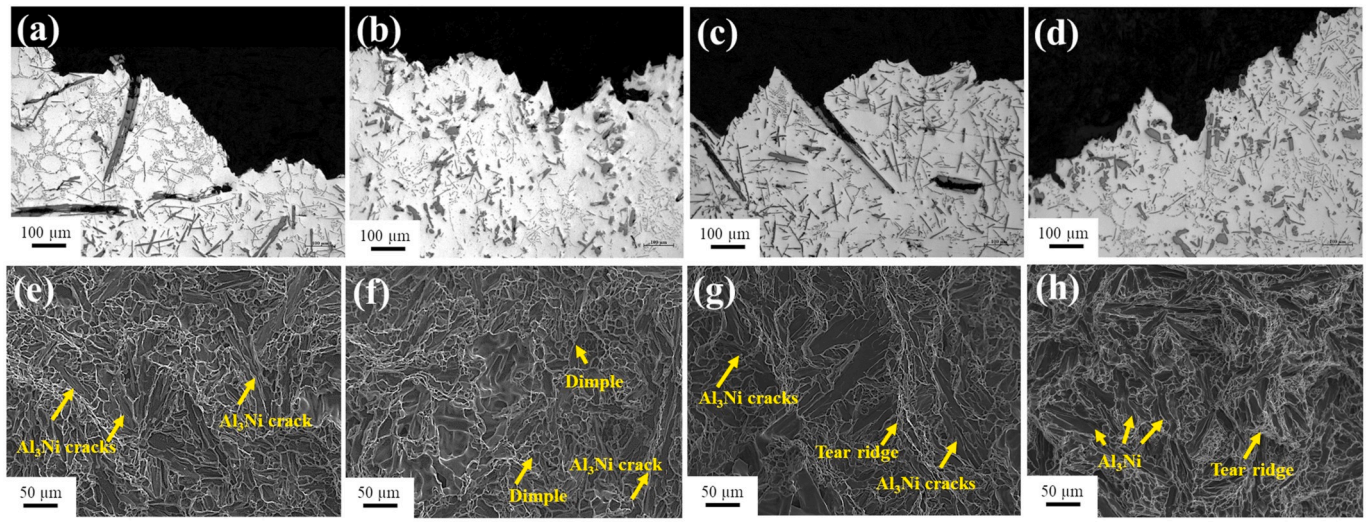

Fig. 13. The analysis of the fracture surface of tensile samples. Optical micrographs of the Al4Fe0·3Zr alloy: (a) as-cast without USP, (b) as-cast with USP, (c) aged without USP, (d) aged with USP. SEM fractography images of the Al8Ni0·3Zr alloy: (e) as-cast without USP, (f) as-cast with USP, (g) aged without USP and (h) aged with USP.

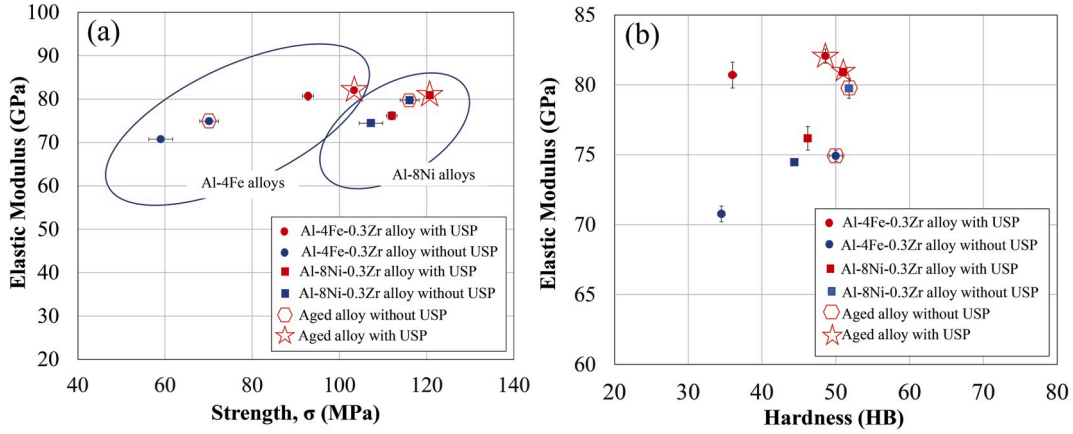

Fig. 14. Comparison of the engineering elastic modulus with strength (b) and hardness (b) of Al–8Fe-0.3Zr and Al8Ni0·3Zr after USP and heat treatment.

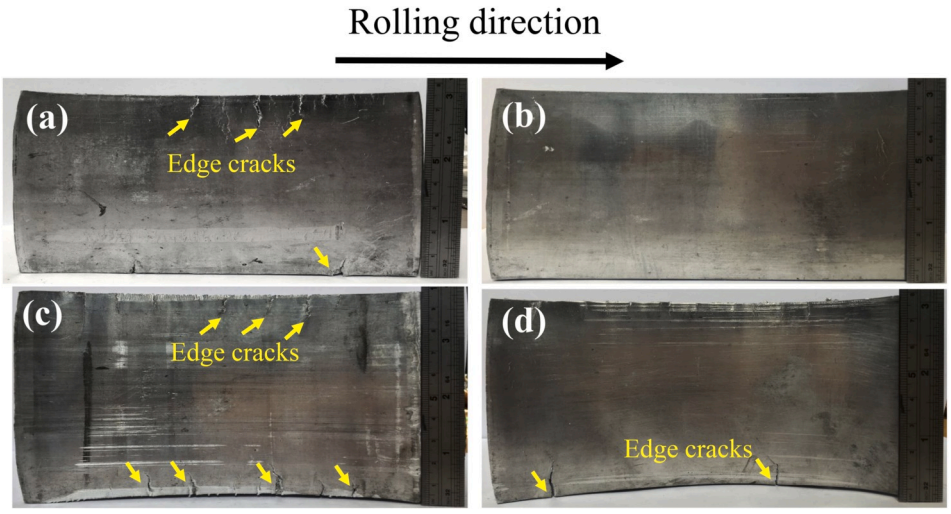

Fig. 15. The surface defects of as-cast samples after 50% deformation by hot process at 400 °C: Al4Fe0·3Zr alloy (a) without USP, (b) with USP, and Al8Ni0·3Zr alloy: (c) without USP and (d) with USP.

large Al_3Fe intermetallics both in cross-section and longitudinal directions.

4. Discussion

4.1. Mechanisms of structure refinement in hypereutectic Al–Fe–Zr and Al–Ni–Zr alloys

It is well known that the formation temperature of primary phases depends on the chemical composition of the alloy as dictated by the phase diagram and conditions of solidification [20]. Thus, we need to choose the temperature range of USP correctly because it has been reported that the treatment temperature plays significant role in the outcome of the structure refinement as it is linked to the structure refinement mechanisms, i.e. nucleation [21] and fragmentation of intermetallics [22]. Our hypothesis was that primary Al_3Zr particles could be refined by USP in the range of their solidification and then affect nucleation of other phases in the alloys, i.e. primary Al_3Ni/Al_3Fe phases and Al/eutectic grains. This hypothesis was based on the previous studies where such effect of the refined Al_3Zr particles was shown for the Al solid solution [15,16], but it was never proved to be working on hypereutectic alloys. The temperature ranges have been selected using the phase diagram calculations as reflecting the primary solidification range of the Al_3Zr phase (Fig. 1) and proved to be selected correctly as Figs. 2 and 3 demonstrate.

The hypothesis was validated. Note that the addition of Zr alone or application of USP only did not result in any significant structure refining effects (see Fig. 2 (c, d) and Fig. 3 (c, d)). The addition of Zr alone produced qualitatively similar structure as the application of USP alone (compare Fig. 2(b) and (d) and Fig. 3(b) and (d). This shows that USP in the alloy without Zr produced (through activation of inclusions as the USP has started above the liquidus, Fig. 1(a and b)) similar amount of nucleation sites as Zr that formed primary (but not refined) Al_3Zr crystals. These crystals were, however, not efficient enough in size and numbers to eliminate completely the columnar structure and refine grains significantly. Only the application of both USP and Zr gives a remarkable structure refining effect (Fig. 2 (e, f) and Fig. 3 (e, f); Fig. 4 (b, d)). The longer the USP and the wider the temperature range of its application, the more pronounced is the effect, which agrees well with earlier research on solid-solution type Al alloys [15].

The mechanisms of structure refinement upon USP of alloys with Zr have been suggested before for the refinement of Al grains [15,16]. These include enhanced nucleation of the primary Al_3Zr phase on activated oxides [23] followed by fragmentation of these primary intermetallics by cavitation [15,16,23]. These refined particles act as solidification sites for the Al solid solution.

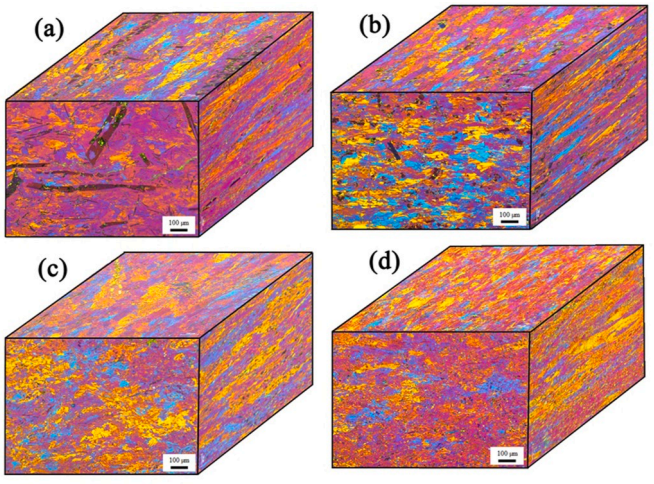

Fig. 16. "3D" microstructure of the deformed samples: (a) Al4Fe0·3Zr-No USP, (b) Al4Fe0·3Zr-USP, (c) Al4Ni0·3Zr-No USP and (d) Al4Ni0·3Zr-USP.

The main structure features of the hypereutectic alloys are, of course, primary intermetallics and eutectic colonies. The results showed that the large Al_3Fe or Al_3Ni particles were not observed after the alloy was treated by USP as shown in Figs. 5 and 6 and in Supplementing Materials. The elimination of large particles is the important effect of USP in both alloys as it has direct consequences in improving the ductility for these hypereutectic alloys.

The observed association of refined primary Al_3Zr particles with Al_3Fe/Al_3Ni intermetallics suggests the possibility of an original (not considered before) refining mechanism, i.e. by the Al_3Zr phase nucleating primary Al_3Fe and Al_3Ni primary crystals (Fig. 8). We understand that these observations are indirect, and the precise mechanisms should be further examined by advanced characterization, which is beyond the scope of the current paper. Yet the fact that Al_3Zr phase forms earlier in solidification than other primary phases (see the red line in Fig. 1) and Al_3Zr phase is observed together with the other primary intermetallics (Figs. 8 and 9 (a, b)) gives enough grounds to suggest the possibility of such a nucleation mechanism.

Furthermore, the occurrence of the refined Al_3Zr particles in the center of eutectic colonies (Figs. 8 and 9 (a, c)) suggests that these particles act as nucleating substrates for the Al solid solution in these colonies and, therefore refine the eutectic grains. This mechanism is quite similar to the previously suggested for Al grains [15,16].

Therefore, the USP-refined Al_3Zr intermetallics may provide the complex structure refinement as shown in Figs. 2–7 and quantified in Table 2. It is demonstrated for the first time that, in addition to acting as nucleation sites for the Al solid solution, these particles may also assist in refining primary Al_3Fe and Al_3Ni intermetallics and eutectic colonies (grains). Therefore, the synergetic effect of USP and Zr is valid for a wider range of alloys than it was previously thought.

4.2. Hardening mechanism

The addition of Zr into alloys had a dual purpose, one to assist the refining the structure with USP (demonstrated above), the other to enable precipitation hardening with the effect preserved at elevated temperatures. Zr tends to retain in the Al solid solution during solidification even at relatively low cooling rates. Thus, formed supersaturated solid solution decomposes at temperatures above 350 °C with precipitation of the metastable Al_3Zr phase that can act as a hardening phase [24]. One may notice from the results in Fig. 10, that the hardness of the alloys subjected to USP was slightly higher than for the alloys without USP in the as-cast state. At the same time, the hardening effect is smaller in the alloys subjected to USP. The former result can be explained from the overall structure refinement and more uniform distribution of hard intermetallics in the structure (see Figs. 6 and 7). The latter observation may be related to the amount of the available Zr in the supersaturated solid solution. This is supported by the measured concentrations that are lower than the theoretical ones as shown in Fig. 11. And the concentrations of Zr in (Al) are also lower in the Al8Ni0·3Zr alloy than in the Al4Fe0·3Zr alloy, and after USP in both alloys. The former may explain a more pronounced hardening in the Al4Fe0·3Zr alloy (Fig. 10). The latter explains why the USP-treated alloys harden less. The smaller amount of Zr available in the solid solution for hardening is a result of more Zr being consumed by the primary Al_3Zr crystals. It has been previously shown by Zhang et al. [11] and Wang et al. [23] that USP facilitates primary solidification of phases through a number of mechanisms, including triggering heterogeneous nucleation on activated oxides always present in the melt. Therefore, USP not only refines the primary particles but also promotes their formation. Nevertheless, even in the case of USP the amount of Zr dissolved in Al is sufficient to reach an adequate hardening level. This is demonstrated by hardness values that are not significantly different for the alloys with or without USP (Fig. 10). Moreover, the results also confirm the precipitation of

metastable $L1_2$ Al_3Zr in Al-matrix as structure as can be seen in Fig. 11 (c). The result is consistent with previous work that investigated the precipitation of Al_3Zr in the Al-matrix, albeit in a solid solution-type alloy [25].

The presence of large volume fraction of intermetallics in combination with refined and uniform structure produced a good combination of tensile properties and rigidity as illustrated in Fig. 14.

4.3. Mechanical properties and feasibility of deformation

USP of Zr-containing hypereutectic alloys led to a considerably increased ductility as can be seen in Figs. 10 and 12. This level of ductility would be beneficial for subsequent forming process. Sufficient ductility was retained after precipitation hardening. This is most likely linked to the achieved significant refining of the as-cast structure that included both primary intermetallics and eutectic colonies (see Figs. 6 and 7).

The achieved ductility in the Al4Fe0·3Zr alloy is higher than in the Al8Ni0·3Zr alloy. This may be related to the fact that USP was most effective in refining the primary intermetallics in the Al–Fe alloys as compared to the Al–Ni alloys where the intermetallics were originally smaller, which is also evidenced by a higher elongation in the latter alloys without USP (see Figs. 6–8 and Table 2). Note also that the eutectic is more uniformly distributed in Al–Ni alloys as compared to the Al–Fe alloys (compare Fig. 8 (b) and (d)), which gives less opportunities for the crack to propagate through ductile Al patches, hence – a lower ductility.

Precipitation hardening with Al_3Zr did not change the character of fracture, with crack propagating through primary intermetallics in the alloy without USP (Fig. 13(c, g)) and through the ductile Al phase in the alloys subjected to USP (Fig. 13(d, h)). This reflects the increase in tensile strength (both UTS and YS) and also the elongation as shown in Fig. 12. The significantly refined upon USP primary intermetallics are not acting as stress concentrators and crack initiators anymore and the fracture goes through the ductile aluminum and eutectic matrix, improving both the ductility and UTS through the delayed fracture. This mechanism agrees well with previous observations [10] that also showed that small, evenly distributed particles can reduce stress concentration in the structure acting as reinforcement in Al-matrix.

The structure refinement and obtained improvement in ductility as a result of USP can make the studied alloys suitable for deformation, which would tremendously increase the range of potential applications. Therefore, we also studied the feasibility of slab forming process by hot rolling. We would like to emphasize again that this study is not about the development and optimization of deformation technology for these typically undeformable alloys, but rather aims at the demonstration of the potential of these alloys to be deformed.

The hot-rolled sheets showed significant cracks in the alloys that were not treated by USP as shown in Fig. 15 (a, c). The alloys subjected to USP demonstrated significantly reduced edge cracking and a smoother surface after rolling (Fig. 15 (b, d)). There is a clear correlation between the improved tensile ductility, the changed mode of fracture (discussed above) and the results of hot rolling. The edge cracks are the result of stress concentration caused by clusters or large individual brittle particles of primary intermetallics as reported by Zhu et al. [26], which may be further facilitated by the drop of temperature at the edges of the slab during rolling as mentioned by McQueen et al. [27].

The existence of large primary intermetallics in the microstructure of the alloys not subjected to USP resulted in the initial crack starting at the microlevel (Fig. 16 (a)) and developing to a macrocrack on the surface as can be seen in Fig. 15 (a, c). Thus, the deformability of hypereutectic Al–Fe and Al–Ni alloys depends on the size and distribution of coarse intermetallics as has been also reported elsewhere for hypoeutectic Al–Fe alloys [28]. USP in combination with Zr additions makes the deformation of these alloys possible due to the refinement of both primary intermetallics and overall “grain” structure.

Although we have not studied the mechanical behavior of the hypereutectic Al–Fe–Zr and Al–Ni–Zr alloys at elevated temperatures, the reference data [4,6,7] gives good indications that such alloys should be superior to Al–Si piston alloys at temperatures above 300 °C.

5. Conclusions

- The structure refinement in hypereutectic Al–Fe and Al–Ni alloys with addition of Zr can be achieved by ultrasonic melt processing in the range of primary solidification of Al_3Zr through fragmentation of primary Al_3Zr particles, which facilitates nucleation processes for other structure constituents. The nucleation of primary Al_3Fe and Al_3Ni phases and dendrites/eutectic grains on the refined Al_3Zr crystals is suggested as a possible mechanism, though this requires further detailed studies.
- Zr retained in the Al solid solution upon solidification of hypereutectic Al–Fe–Zr and Al–Ni–Zr alloys enables the precipitation hardening by coherent metastable Al_3Zr nano-particles. USP facilitates the formation of primary Al_3Zr phase and decreases somewhat the level of Zr in the solid solution that, however, remains sufficient for precipitation hardening.
- The strength and ductility of the hypereutectic alloys can be significantly improved by structure refinement upon USP; and the ductility level remains sufficiently high after precipitation hardening. The fracture mode changes from brittle to ductile.
- The level of ductility achieved in the as-cast hypereutectic alloys after USP makes possible hot deformation of these alloys.

Data availability statement

The raw/processed data required to reproduce these findings cannot be shared at this time as the data also forms part of an ongoing study.

Declaration of competing interest

The authors declare that they have no known competing financial interests or personal relationships that could have appeared to influence the work reported in this paper.

CRediT authorship contribution statement

Suwaree Chankitmunkong: Methodology, Data curation, Validation, Formal analysis, Investigation, Writing - original draft. **Dmitry G. Eskin:** Conceptualization, Methodology, Resources, Supervision, Investigation, Writing - review & editing, Funding acquisition. **Chaowalit Limmaneevichitr:** Supervision, Validation, Writing - review & editing, Funding acquisition.

Acknowledgements

The authors gratefully acknowledge King Mongkut’s University of Technology Thonburi for funding Postdoctoral Fellowship to S.C., and the financial support from the “KMUTT 55th Anniversary Commemorative Fund” is also acknowledged by S.C. and C.L. D.E. acknowledges the financial support from EPSRC (UK) under project UltraMelt2 (EP/R011001/1, EP/R011044/1 and EP/R011095/1). We also grateful to Dr F. Wang of BCAST for help in performing TEM studies.

Appendix A. Supplementary data

Supplementary data to this article can be found online at https://doi.org/10.1016/j.msea.2020.139567.

References

[1] J. Jorstad, D. Apelian, Hypereutectic Al-Si alloys: practical casting considerations, Int. J. Metalcast. 3 (3) (2009) 13–36, https://doi.org/10.1007/BF03355450.

[2] J.M. Cubero-Sesin, Z. Horita, Strengthening of Al through addition of Fe and by processing with high-pressure torsion, J. Mater. Sci. 48 (13) (2013) 4713–4722, https://doi.org/10.1007/s10853-012-6935-8.

[3] M.F. Kilicaslan, E. Karakose, Depth sensing indentation analyses of hypereutectic Al-10Ni-XSc (X = 0, 1, 2) alloys, Met. Mater. Int. 23 (3) (2017) 473–480, https://doi.org/10.1007/s12540-017-6686-9.

[4] N.A. Belov, Aluminium casting alloys with high content of zirconium, Mater. Sci. Forum, Trans Tech Publ. 217–222 (1996) 293–298. https://doi.org/10.4028/www.scientific.net/MSF.217-222.293.

[5] C. Suwanpreecha, P. Pandee, U. Patakham, C. Limmaneevichitr, New generation of eutectic Al-Ni casting alloys for elevated temperature services, Mater. Sci. Eng., A 709 (2018) 46–54, https://doi.org/10.1016/j.msea.2017.10.034.

[6] N. Belov, V.S. Zolotorevskii, Casting alloys on the base of aluminium-nickel eutectic (nikalines) as possible alternative to silumins, Tsvetnye Met. (2) (2003) 99–105.

[7] D.G. Eskin, L. Toropova, Tensile and elastic properties of deformed heterogeneous aluminum alloys at room and elevated temperatures, Mater. Sci. Eng., A 183 (1–2) (1994) L1–L4, https://doi.org/10.1016/0921-5093(94)90913-X.

[8] Z. Ma, A.M. Samuel, H.W. Doty, S. Valtierra, F.H. Samuel, Effect of Fe content on the fracture behaviour of Al–Si–Cu cast alloys, Mater. Des. 57 (2014) 366–373, https://doi.org/10.1016/j.matdes.2014.01.037.

[9] N.A. Belov, A.A. Aksenov, D.G. Eskin, Iron in Aluminium Alloys: Impurity and Alloying Element, CRC Press, Boca Raton, 2002.

[10] S.X. Luo, Z.M. Shi, N.Y. Li, Y.M. Lin, Y.H. Liang, Y.D. Zeng, Crystallization inhibition and microstructure refinement of Al-5Fe alloys by addition of rare earth elements, J. Alloys Compd. 789 (2019) 90–99, https://doi.org/10.1016/j.jallcom.2019.03.071.

[11] L. Zhang, D. Eskin, L. Katgerman, Influence of ultrasonic melt treatment on the formation of primary intermetallics and related grain refinement in aluminum alloys, J. Mater. Sci. 46 (15) (2011) 5252–5259, https://doi.org/10.1007/s10853-011-5463-2.

[12] G.I. Eskin, D.G. Eskin, Ultrasonic Treatment of Light Alloy Melts, CRC Press, Boca Raton, 2015.

[13] S. Chankitmunkong, D.G. Eskin, C. Limmaneevichitr, Microstructure evolution in an Al-Si piston alloy under ultrasonic melt processing, in: IOP Conference Series: Materials Science and Engineering, IOP Publishing, 2019, 012060, https://doi.org/10.1088/1757-899X/529/1/012060.

[14] W. Khalifa, Y. Tsunekawa, M. Okumiya, Effect of ultrasonic treatment on the Fe-intermetallic phases in ADC12 die cast alloy, J. Mater. Process. Technol. 210 (15) (2010) 2178–2187, https://doi.org/10.1016/j.jmatprotec.2010.08.008.

[15] T. Atamanenko, D. Eskin, L. Zhang, L. Katgerman, Criteria of grain refinement induced by ultrasonic melt treatment of aluminum alloys containing Zr and Ti, Metall. Mater. Trans. 41 (8) (2010) 2056–2066, https://doi.org/10.1007/s11661-010-0232-4.

[16] T.V. Atamanenko, D.G. Eskin, M. Sluiter, L. Katgerman, On the mechanism of grain refinement in Al–Zr–Ti alloys, J. Alloys Compd. 509 (1) (2011) 57–60, https://doi.org/10.1016/j.jallcom.2010.09.046.

[17] K.E. Knipling, D.N. Seidman, D.C. Dunand, Ambient- and high-temperature mechanical properties of isochronally aged Al–0.06Sc, Al–0.06Zr and Al–0.06Sc–0.06Zr (at.%) alloys, Acta Mater. 59 (3) (2011) 943–954, https://doi.org/10.1016/j.actamat.2010.10.017.

[18] N. Belov, A. Alabin, D. Eskin, Improving the properties of cold-rolled Al–6% Ni sheets by alloying and heat treatment, Scripta Mater. 50 (1) (2004) 89–94, https://doi.org/10.1016/j.scriptamat.2003.09.033.

[19] K.E. Knipling, R.A. Karnesky, C.P. Lee, D.C. Dunand, D.N. Seidman, Precipitation evolution in Al–0.1Sc, Al–0.1Zr and Al–0.1Sc–0.1Zr (at.%) alloys during isochronal aging, Acta Mater. 58 (15) (2010) 5184–5195, https://doi.org/10.1016/j.actamat.2010.05.054.

[20] L.F. Mondolfo, Aluminum Alloys: Structure and Properties, Butterworths, Boston, 1976.

[21] F. Wang, D. Eskin, J. Mi, T. Connolley, J. Lindsay, M. Mounib, A refining mechanism of primary Al $_3$Ti intermetallic particles by ultrasonic treatment in the liquid state, Acta Mater. 116 (2016) 354–363, https://doi.org/10.1016/j.actamat.2016.06.056.

[22] J.Y. Wang, B.J. Wang, L.F. Huang, Structural evolution of Al–8%Si hypoeutectic alloy by ultrasonic processing, J. Mater. Sci. Technol. 33 (11) (2017) 1235–1239, https://doi.org/10.1016/j.jmst.2017.07.018.

[23] F. Wang, D. Eskin, T. Connolley, J. Mi, Influence of ultrasonic treatment on formation of primary Al_3Zr in Al–0.4Zr alloy, Trans. Nonferrous Metals Soc. China 27 (5) (2017) 977–985, https://doi.org/10.1016/S1003-6326(17)60115-8.

[24] K.E. Knipling, R.A. Karnesky, C.P. Lee, D.C. Dunand, D.N. Seidman, Precipitation evolution in Al–0.1 Sc, Al–0.1 Zr and Al–0.1 Sc–0.1 Zr (at.%) alloys during isochronal aging, Acta Mater. 58 (15) (2010) 5184–5195, https://doi.org/10.1016/j.actamat.2010.05.054.

[25] S.Y. Jiang, R.H. Wang, Manipulating nanostructure to simultaneously improve the electrical conductivity and strength in microalloyed Al-Zr conductors, Sci. Rep. 8 (1) (2018) 6202, https://doi.org/10.1038/s41598-018-24527-4.

[26] Y.Z. Zhu, Q. Wan, B.l. Li, F. Zhou, Y.F. Zhang, Three-dimensional modeling of effect of surface intermetallic phase on surface defects of Al–Fe–Si aluminum foils during twin-roll casting, Trans. Nonferrous Metals Soc. China 24 (2) (2014) 477–483, https://doi.org/10.1016/S1003-6326(14)63085-5.

[27] H.J. McQueen, S. Spigarelli, M.E. Kassner, E. Evangelista, Hot Deformation and Processing of Aluminum Alloys, CRC Press, Boca Raton, 2016.

[28] P.R. Goulart, V.B. Lazarine, C.V. Leal, J.E. Spinelli, N. Cheung, A. Garcia, Investigation of intermetallics in hypoeutectic Al–Fe alloys by dissolution of the Al matrix, Intermetallics 17 (9) (2009) 753–761, https://doi.org/10.1016/j.intermet.2009.03.003.